Definition of the mechanical design parameters to optimize efficiency of integral force feedback active damping strategy

Philippe Monnier-Benoit, Manuel Collet, Jean Piranda

Definition of mechanical design parameters to optimize efficiency of integral force feedback

P. Monnier, M. Collet*,y and J. Piranda

Laboratoire de Mécanique Appliquée R. Chaléat, 24 rue de l'Epitaphe, 25000 Besançon, France

Collocated IFF control strategy is commonly used thanks to its strong quality of robustness, which is due to its intrinsic damping property. Up to now, the extensive studies available in the literature have focused only on the obtained mechanical efficiency in terms of modal damping ratios. We propose here to exhibit some mechanical design parameters allowing one to really optimize this dissipation strategy, not only in terms of induced damping, but also in terms of control signal magnitudes. We apply our criterion to two different plate systems to emphasize the effects of such design variables on the control implementation. At the end, we demonstrate how the best designed system can be coupled with a non-centralized approach to increase the implementation efficiency.

KEY WORDS: structural collocated control; integral force feedback (IFF); plate; optimization

1. INTRODUCTION

Although active control has been widely studied to stabilize simple mechanical structures such as beams [1–3], plates [4–6] or shells [7,8] during the past ten years, its application on industrial structures has been hindered by the complexity of its implementation and the lack of robust efficiency [9–11]. The main drawback resides in the difficulty to apply the classical results of automatics to some distributed structures with an infinite number of degrees of freedom. Model-based approaches such as the LQ-family always introduce non-modeled dynamic uncertainties leading to spillover instabilities and lack of robustness [10,12]. New strategies based on convex optimization allow one to overcome these difficulties by introducing uncertainties as new constrains based on LMI (linear matrix inequalities) [13]. In this case, some examples show up a lack of control efficiency because of the mathematical difficulties of such an optimization [14].

Following the earlier work of J. L. Lions [15] on the exact controllability of partial differential equations, some new strategies dedicated to the control of mechanical structures have been developed. For example the Komornik feedback law [16–18] has been introduced. This strategy induces a very fast decay rate of energy and imposes an exponential stability to flexible

*Correspondence to: M. Collet, Laboratoire de Mécanique Appliquée R. Chaléat, 24 rue de l'Épitaphe, 25000 Besançon, France.
† E-mail: manuel.collet@univ-fcomte.fr

structures. This very efficient method, experimentally implemented on a beam [19], has shown its capability to outperform classical obtained results on such a structure. Unfortunately, the robust stability is not yet quantified and problem of spillover may occur.

The only intrinsically robust strategies are the collocated active damping methods such as direct velocity feedback [20,21] and its dual counterpart, integral force feedback [11,22,23]. In its theoretical form, this control appears as a simple damping system with all the properties of robust stability that prevent it from spillover effects. However, the problem may occur in practice because of either sensor and actuator dynamics, or the difficulty to achieve collocation properly. Moreover, this non-optimal strategy may lack efficiency because of the spatial localization of the damping effect and the necessary low- or high-pass filtering which strongly deteriorates the performances.

Our purpose is to exhibit sensitive design parameters to optimize IFF efficiency in stabilizing flexible structures. To complement the results obtained by A. Preumont [11], we precisely define, in a first part, our mechanical design criterion. It not only appears as a function of the induced mechanical stability, but also as a function of the control signal magnitude. In a second part, we confirm our first results by studying the efficiency of IFF in controlling two different plate systems. We show the validity of our optimal design criterion by numerical results and moreover through experimental measurements. At last we show how to increase efficiency by introducing a decentralized approach.

2. THEORETICAL APPROACH OF IFF

2.1. Introduction

Collocated active control stands out from other control strategies by the localization of the sensor and the actuator at the same point in the structure, these devices measuring two dual quantities. Two different classes of collocated active damping coexist: the integral force feedback (IFF) strategy and its dual version, the direct velocity feedback (DVF) strategy.

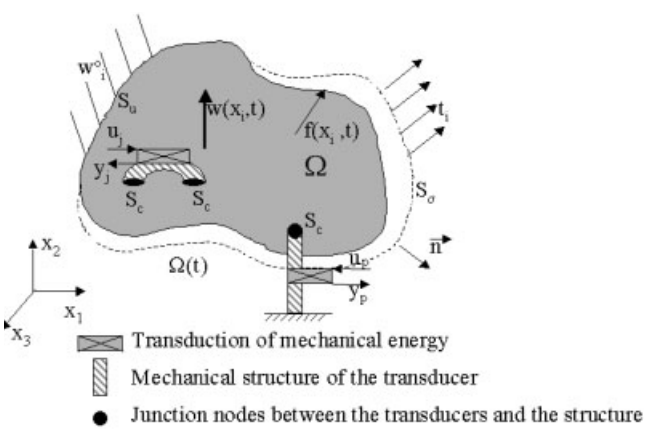

Figure 1. Mechanical system controlled by collocated strategies.

Consider Figure 1 composed of a mechanical system equipped with both inner and outer transducers. Suppose we measure a force F at a point of the mechanical system and we impose at the same point the dual displacement u^{d} such that:

$$u^{\mathrm{d}}(t) = -g \int F(t)\,\mathrm{d}t \qquad g \in \mathbb{R}^{+} \tag{1}$$

then the mechanical power injected into the system can be written:

$$P(t) = F(t)\dot{u^{\mathrm{d}}}(t) = -gF^2(t) \leqslant 0 \tag{2}$$

As it is negative, we have thus introduced a dissipation of energy on the structure by the IFF strategy. The dissipated energy is then proportional to the integral of the squared force F supported by the transducer. As we will demonstrate later in this paper, this force increases as the system becomes increasingly mechanically constrained by the transducers. IFF control is thus more efficient when the actuator is stiff with respect to the structure.

On the contrary, if we measure a velocity $\dot{w}$ and inject at the same point of the structure its dual effort u^{f} such that:

$$u^{\mathrm{f}}(t) = -g\dot{w}(t) \qquad g \in \mathbb{R}^{+} \tag{3}$$

then the power injected into the system can be written:

$$P(t) = u^{\mathrm{f}}(t)\dot{w}(t) = -g\dot{w}^2(t) \leqslant 0 \tag{4}$$

Here, the dissipated power is proportional to the square of the structure velocity at the control point. Unlike the IFF strategy, the DVF strategy is more efficient if the structure is weakly constrained by the transducers and can conveniently be used when the transduction system has a small mechanical impedance.

Both collocated strategies are unconditionally stable in their theoretical version. As Equations (2) and (4) clearly show, the power brought to the structure is negative, so that the energy of the mechanical system under control always decreases, and no spillover effect can occur.

Within the next sections, we will investigate the main characteristics of IFF to underline design variables enabling the optimization of this non-optimal control strategy. Then we will apply it to damp the transversal vibrations of a plate with different sets of boundary conditions and control architectures.

2.2. Properties of the IFF strategy

First we should model each transduction element appropriately, and underline the mechanical assumptions used.

Consider the transducer made of a force sensor with stiffness k_{c} and of a piezoelectric actuator with stiffness k_{a} connected in series, as shown in Figure 2. Both devices can be modeled as simple beams with two degrees of freedom, with length L and section A, working in extension along the third direction z. As flexural movements are uncontrollable, they are not mentioned here, although they are directly introduced via the beam element. By using IEEE vector notations, tension stress T_3 and strain S_3 are coupled with the electric field z-component E_3 according to the piezoelectric effect:

$$T_3 = c_{33}S_3 - e_{33}E_3 \tag{5}$$

where c_{33} is the Young's Modulus and e_{33} a piezoelectric coupling coefficient.

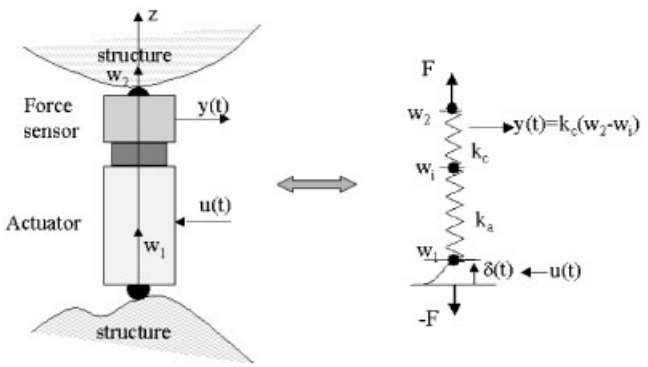

Figure 2. Transduction system.

First, let us consider the second term of Equation (5). The electrical field E is linked to the electrical potential V at the electrodes of each layer by the relation $E = -\text{grad}(V)$. We deduce the first approximation:

$$E_3 = -n\frac{V}{L} \tag{6}$$

where n is the number of piezoelectric layers and L the length of the stack.

According to the characteristics of a piezoelectric material, e_{33} can be written as a function of the coupling coefficient d_{33}:

$$e_{33} = 2d_{31}c_{31} + d_{33}c_{33} \approx d_{33}c_{33} \tag{7}$$

Then Equation (5) becomes:

$$T_3 = c_{33}S_3 + nc_{33}d_{33}\frac{V}{L} = c_{33}\left(S_3 + \frac{\delta}{L}\right) \tag{8}$$

where $\delta = nd_{33}V$ is the extension of the piezoelectric stack imposed by the applied voltage. To discretize the problem, we can use a linear, first-order interpolation function:

$$w(z) = \frac{1-z}{L}w_1 + \frac{z}{L}w_2 \tag{9}$$

where w_1 and w_2 are the nodal displacements of the rod.

According to the theory of rods, the normal force F is linked to the strain $S_3 = \mathrm{d}w/\mathrm{d}z$ by the relation:

$$F = \frac{e_{33}A}{L}\frac{\mathrm{d}w}{\mathrm{d}z} = k\frac{\mathrm{d}w}{\mathrm{d}z} \tag{10}$$

Then, static equilibrium can be written at each degree of freedom introduced on Figure 2:

$$k_\mathrm{a}w_2 - k_\mathrm{a}w_\mathrm{i} + k_\mathrm{a}\delta = F \tag{11a}$$

$$-k_\mathrm{a}w_2 + (k_\mathrm{a} + k_\mathrm{c})w_\mathrm{i} - k_\mathrm{c}w_1 = 0 \tag{11b}$$

$$k_\mathrm{c}w_\mathrm{i} - k_\mathrm{c}w_1 = -F \tag{11c}$$

where w_1 and w_2 are the external degrees of freedom of the transducer (sensor + actuator), w_i the internal degree of freedom modelling the connection between the sensor and the actuator, and F the force applied by the transducer.

Then, by eliminating the internal variable w_i from Equation (11b) and replacing it in Equations (11a) and (11c), the force applied by the transducer to the connected structure can be written:

$$F = -\frac{k_a k_c}{k_c + k_a}(w_2 - w_1 - \delta) = -k_e(w_2 - w_1) - k_e\delta = F_m + F_p \tag{12}$$

As mentioned before, k_a is the actuator stiffness, k_c the sensor stiffness and so k_e is classically the passive system equivalent stiffness. Note that F_p, the part of the force due to the piezoelectric effect, is the product of the equivalent stiffness k_e by the displacement δ imposed to the actuator.

Inertial terms have been neglected. This non-causal approach (two springs in serial connection) is of course very approximative, particularly to deal with high-frequency stability problems related to the inner dynamics of the transducer. A simple Guyan condensation of the neglected inertial terms could be made to introduce mass terms on degrees of freedom w_1 and w_2.

The displayed scheme symbolizes the control of only one degree of freedom. If the transducer acts on several degrees of freedom, a coupling matrix must be introduced into the model. We find this kind of simplified approach in the vast majority of works on IFF control [11,24]. It allows one to establish easily the major characteristics of the method without entering the details of the multi-physical coupling peculiar to energy transduction.

Now, consider a mechanical structure and a transducer with equivalent stiffness k_e. Let M_s, K_s be the mass and stiffness matrices of the structure, and M, K the mass and stiffness matrices of the whole system with the transducer. Thus, matrix K represents the structural stiffness augmented with that of the transducer: $K = K_s + b^T k_e b$, where b is an influence matrix locating the transducer within the structure. Note that the measurement y made by the force sensor is opposite to the force F applied by the actuator to the structure, so $y = k_e(w_2 - w_1 - \delta)$. Then the set of linear equations describing the dynamical equilibrium of the homogeneous system can be written:

$$M\ddot{w} + Kw = bk_e\delta \tag{13}$$

$$y = k_e(b^T w - \delta) \tag{14}$$

or in term of Laplace variables:

$$(s^2 M + K)\tilde{w} = bk_e\tilde{\delta} \tag{15}$$

$$\tilde{y} = k_e(b^T\tilde{w} - \tilde{\delta}) \tag{16}$$

With no loss of generality, we can consider the same structure with a set of n transducers, each one identical to that described previously. In the following, to simplify the notation, we substitute to the equivalent transducer stiffness k_e, the diagonal matrix made of the equivalent stiffnesses of all transducers. Equation (13) still stands, but δ now represents the vector of the displacements imposed by each actuator, and b is a rectangular matrix with as many columns as transducers connected to the structure. For the same reason of simplification, functions $w(t)$, $\delta(t)$, $y(t)$ and their Laplace transform previously noted $\tilde{w}(s)$, $\tilde{\delta}(s)$, $\tilde{y}(s)$ will be associated with w, δ, y.

The IFF control law directly relates inputs and outputs of the system via an integrator filter:

$$\delta = k_e^{-1} \frac{G}{s} y \tag{17}$$

The control feedback gain matrix $G \in \mathbb{R}^n$ must be semi-positive definite in order to ensure the controlled system stability as in Equation (1). This matrix is not necessarily symmetrical. Two cases can be encountered:

- If G is diagonal, the control is said to be decentralized, as all transducers are autonomous and do not communicate with each other. This is obviously a convenient case if, by implementing the control law, one wishes to economize on multichannel addressing by localizing the controller on each transduction system.
- If G is full, the control is centralized. Each actuator uses measurements from the whole set of sensors and not only that of the corresponding collocated sensor.

Previous work [11] has shown the behavior of such a system as a function of G. Eliminating y from Equations (16) and (17), then substituting δ in (15) leads to the equation ruling the homogeneous controlled system behavior in Laplace space:

$$[s^2 M + (K - bk_e(sI + G)^{-1} G b^T)]w = 0 \tag{18}$$

So when $\|G\| \to +\infty$, Equation (18) becomes:

$$[s^2 M + (K - bk_e b^T)]w = 0 \tag{19}$$

This is the equation of motion of the homogeneous system without any transducer: the associated stiffness matrix, $K - bk_e b^T$, is that of the structure alone K_s. If the transducers have a high mechanical impedance, we will pass, as G increases, from a system with Dirichlet conditions (almost clamped) on the connexion points when $\|G\| = 0$ to a free system when $\|G\| \to +\infty$.

2.3. Sensitivity

At this point we will study the sensitivity of the induced modal damping to the gain of the IFF controller in order to underline some important design variables. From Equations (15), (16) and (17), we can describe the controlled system behavior according to (20):

$$\begin{bmatrix} s^2 M + K & -bk_e \\ -Gb^T & (sI_n + G) \end{bmatrix} \begin{bmatrix} w \\ \delta \end{bmatrix} = 0 \tag{20}$$

Here I_n is the identity matrix in $\mathbb{R}^n$. We assume that the feedback gain matrix G is a diagonal matrix with a single gain: $G = gI_n$. This means that a completely decentralized system with only one common gain g is considered. This simple form will allow us to analyze analytically the sensitivity of the system.

We first project the first equation of the homogeneous problem (Equation (20)) on the eigenvector basis of the uncontrolled system (the mechanical structure with the transducers and $g = 0$). Let $(\{\phi_i, \Omega_i^2\})_{i=1\ldots N}$ be the eigenproblem solutions (eigenvectors and eigenvalues) that are regrouped in the matrix form (ϕ, Ω^2). Then, by introducing the change of variables $w = \phi z$,

the problem related to (Equation (20)) becomes:

$$\begin{bmatrix} s^2 I_N + \Omega^2 & -\phi^{\mathrm{T}} b k_{\mathrm{e}} \\ -g b^{\mathrm{T}} \phi & (s+g) I_n \end{bmatrix} \begin{bmatrix} z \\ \delta \end{bmatrix} = 0 \tag{21}$$

The coupled equation system can be rewritten by separating variables z and δ:

$$[s^3 I_N + g s^2 I_N + s\Omega^2 + g(\Omega^2 - \phi^{\mathrm{T}}(b k_{\mathrm{e}} b^{\mathrm{T}})\phi)]z = 0 \tag{22}$$

$$[-g b^{\mathrm{T}} \phi (s I_N + \Omega^2)^{-1} \phi^{\mathrm{T}} b k_{\mathrm{e}} + (s+g) I_n]\delta = 0 \tag{23}$$

Both matrix equations obtained above are non-diagonal because of the coupling terms $\phi^{\mathrm{T}}(b k_{\mathrm{e}} b^{\mathrm{T}})\phi$ and $b^{\mathrm{T}}\phi(s I_N + \Omega^2)^{-1}\phi^{\mathrm{T}} b$. A simplification commonly made [11] is to diagonalize Equation system (21). But these coupling matrices can not be considered even to be diagonally dominant for high gain g. In fact the theoretical root locus in Figure 3 obtained by neglecting nondiagonal terms of the coupling matrix is only closed to the real one when g is near zero and differs drastically as g increases. So we will only consider the small gain effect for which simple results can be obtained.

In that purpose, we now study the sensitivity of the controlled system poles to the variations of gain g around zero. At this step, we can distinguish in the full matrix $\phi^{\mathrm{T}}(b k_{\mathrm{e}} b^{\mathrm{T}})\phi$ of Equation (22) the diagonal from the rest, by rewriting it appropriately:

$$\phi^{\mathrm{T}}(b k_{\mathrm{e}} b^{\mathrm{T}})\phi = \mathrm{diag}(v_i \Omega_i^2) + R \tag{24}$$

where v_i is the fraction of strain energy as introduced in [11] and R a symmetrical matrix with zero diagonal terms. We also introduce the modified modal pulsation matrix $\omega = \mathrm{diag}(\omega_i)$ such that:

$$\omega_i^2 = \Omega_i^2(1 - v_i) = \Omega_i^2 - \mathrm{diag}(\phi^{\mathrm{T}}(b k_{\mathrm{e}} b^{\mathrm{T}})\phi) \tag{25}$$

When $g \to +\infty$, the system poles move on a loop in the left half-plane, departing from the poles of the uncontrolled structure Ω_{m}, and going to the poles of the mechanical structure without transducer Ω_{m}^s (Figure 3). Note that the latter poles are very different from the modified pulsations ω_i, particularly when the actuator stiffness k_{e} is high compared with the system stiffness.

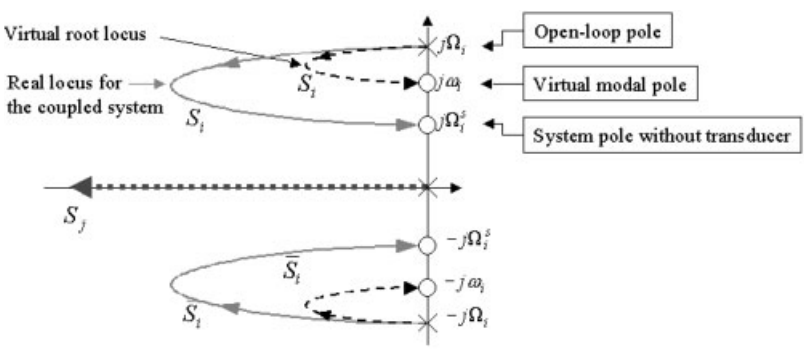

Figure 3. Root locus of modal state Equations (22) and (21).

The poles are the roots of the determinant of Equations (22) and (23). By slightly modifying Equation (22), we thus obtain the characteristic equations of the system (26) and (27).

$$H_1(s,g) = \det(s^3 I_N + g s^2 I_N + s\Omega^2 + g(\Omega^2 - \phi^{\mathrm{T}}(b k_{\mathrm{e}} b^{\mathrm{T}})\phi)) = 0 \tag{26a}$$

or taking Equation (24) into account:

$$= \det(s^3 I_N + g s^2 I_N + s\Omega^2 + g\omega^2 - gR) = 0 \tag{26b}$$

$$H_2(s,g) = \det(-g b^{\mathrm{T}} \phi (s^2 I_N + \Omega^2)^{-1} \phi^{\mathrm{T}} b k_{\mathrm{e}} + (s+g) I_n) = 0 \tag{27}$$

Equation (26) describes the evolution of the N mechanical modes of the system, whereas Equation (27) governs the n poles related to the controller. Let us examine the sensitivity of all initial roots as a function of g, around $g = 0$.

Let s_{p} be the family of the system poles at first order in g:

$$s_{\mathrm{p}} = \{s_{\mathrm{m}_i}, s_{\mathrm{c}_j}\}$$

and s_{p}^0 that of the poles of the uncontrolled system ($g = 0$):

$$s_{\mathrm{p}}^0 = \{s_{\mathrm{m}_i}^0, s_{\mathrm{c}_j}^0\} = \{\{\pm j\Omega_i\}_{i=1\ldots N}, \{0\}_{j=1\ldots n}\}$$

The n poles s_{c_j} are the n controller integration poles. The $2N$ other poles s_{m_i} represent the mechanical eigenfrequencies, arranged in N pairs of complex conjugate values.

The mechanical poles are the solutions of the implicit equation $H_1(s,g) = \det(H) = 0$. The sensitivity of the mechanical poles s_{m_i} to the variations of g is then given by:

$$\frac{\mathrm{d}s}{\mathrm{d}g}(0) = -\left.\frac{\partial H_1(s,g)/\partial g}{\partial H_1(s,g)/\partial s}\right|_{\substack{s = s_{\mathrm{m}_i}^0 \\ g = 0}} \tag{28}$$

According to the expression of the determinant H_1 can be written:

$$H_1 = \sum_{\sigma \in S_n} \varepsilon(\sigma) \prod_{i=1}^{N} H_{i\sigma(i)}$$

where σ is the permutation on the columns of H and $\varepsilon(\sigma)$ the signature of σ. Note that in H_1 all matrix terms are diagonal except matrix R, so that all off-diagonal terms of H are the off-diagonal terms of gR. As the permutation is a bijection on the columns of H, at least two off-diagonal terms R_{ij} may be present in the product $\prod_{i=1}^{N} H_{i\sigma(i)}$. So all terms of the determinant H_1 involving off-diagonal terms induced by matrix gR are thus all proportional to monomial g^k with $k \geqslant 2$. These terms are not simplified by division in the rational fraction (28). Then, when $s = s_{\mathrm{m}_i}^0 \neq 0$, all terms of R are canceled when $g = 0$. Thus we can omit this matrix in the calculation of the sensitivity.

Consider $\tilde{H}_1(s,g) = \det(s^3 I + g s^2 I + s\Omega^2 + g\omega^2)$. As we have previously mentioned,

$$\frac{\partial H_1(s,g)}{\partial g}\Big|_{g=0} = \frac{\partial \tilde{H}_1(s,g)}{\partial g}\Big|_{g=0}$$

Obviously, as matrix gR does not depend on s,

$$\frac{\partial H_1(s,g)}{\partial s}\Big|_{g=0} = \frac{\partial \tilde{H}_1(s,g)}{\partial s}\Big|_{g=0}$$

so Equation (28) becomes:

$$\left.\frac{\mathrm{d}s}{\mathrm{d}g}\right|_{\substack{s=s^0_{\mathrm{m}_i}\\ g=0}} = -\frac{\sum_{k=1}^{N}(s^{02}_{\mathrm{m}_i}+\omega_k^2)\prod_{l\neq k}(s^{02}_{\mathrm{m}_i}+\Omega_l^2)}{\sum_{k=1}^{N}(3s^{02}_{\mathrm{m}_i}+\Omega_k^2)\prod_{l\neq k}(s^{02}_{\mathrm{m}_i}+\Omega_l^2)} \tag{29}$$

We deduce the expression of evolution of the mechanical poles of the controlled system near $g = 0$, at first order in g:

$$s^0_{\mathrm{m}_i} = -g\frac{\Omega_i^2-\omega_i^2}{2\Omega_i^2} \pm j\Omega_i \tag{30}$$

For Equation (27), the problem is slightly different. The expression of sensitivity (Equation (28)) applied to H_2 is undetermined at the initial point corresponding to the pole of the integral operator: $s = 0$ and $g = 0$, as numerator and denominator cancel each other. In this case, the monomial terms of type g^k associated to the non-diagonal terms of $b^{\mathrm{T}}\phi(sI_N+\Omega^2)^{-1}\phi^{\mathrm{T}}b$ can't be simplified *a priori* because they will participate to the limit of the sensitivity as $g \to 0$.

To overcome this problem, we first show that:

$$\begin{aligned}&\mathrm{d}(\det(-gb^{\mathrm{T}}\phi(s^2I_N+\Omega^2)^{-1}\phi^{\mathrm{T}}bk_{\mathrm{e}}+(s+g)I_n))|_{s=0}\\ &=\mathrm{d}(\det(-gb^{\mathrm{T}}\phi\Omega^{-2}\phi^{\mathrm{T}}bk_{\mathrm{e}}+(s+g)I_n))\end{aligned} \tag{31}$$

According to the orthogonality of the natural modes on M and K, we prove that $\phi(\Omega^{-2})\phi^{\mathrm{T}} = K^{-1}$. Matrix K^{-1} is called the static compliance operator. Then Equation (27) becomes:

$$\begin{aligned}&\mathrm{d}(\det(-gb^{\mathrm{T}}\phi(s^2I_N+\Omega^2)^{-1}\phi^{\mathrm{T}}bk_{\mathrm{e}}+(s+g)I_n))|_{s=0}\\ &=\mathrm{d}(\det(-gk_{\mathrm{e}}(b^{\mathrm{T}}K^{-1}b)+(s+g)I_n))|_{s=0}\\ &=0\end{aligned} \tag{32}$$

We finally project the eigenvalue problem associated to the previous characteristic Equation (32) on the basis of the eigenvectors of the square symmetrical matrix $b^{\mathrm{T}}K^{-1}b \in \mathbb{R}^{n\times n}$. Let $\psi \in \mathbb{R}^{n\times n}$ be the matrix of mode shapes, $L \in \mathbb{R}^{n\times n}$ the diagonal matrix of eigenvalues, solutions of the eigenproblem of (Equation (33)), normalized so that $\psi^{\mathrm{T}}\psi = I_n$:

$$b^{\mathrm{T}}K^{-1}b\psi = \psi L \tag{33}$$

The operator $b^{\mathrm{T}}K^{-1}b$ is the Neumann–Dirichlet operator or the Schur dual complement [25] associated with the distribution of the transducers on the mechanical structure. The eigenvalues solution of the characteristic equation $\det(-gk_{\mathrm{e}}(b^{\mathrm{T}}K^{-1}b)+(s+g)I_n) = 0$ are also solution of

$\det(-gk_e L + (s+g)I_n) = 0$. In this simple case, it comes:

$$\left.\frac{ds}{dg}\right|_{\substack{g=0 \\ s=s_{c_j}^0}} = k_e L_j - 1 \tag{34}$$

From Equation (34) we deduce the first-order evolution (in g) of the n poles associated with the control:

$$s_{c_j}^0 = g(k_e L_j - 1) \tag{35}$$

The poles $s_{c_j}^0$ are related to the response of the n integrators used to compute the control signal. They must remain strictly negative in order to guarantee the system stability. In order to limit the level of the imposed displacement δ, we should maximize $|s_{c_j}^0|_{j=1\ldots n}$. The closer to $1/k_e$ eigenvalues L_j will be, the less the energy decay rate of the control signal will be, and the higher the associated control displacement δ will be. These eigenvalues, regrouped in the matrix $L = \mathrm{diag}(L_i)_{i=1\ldots n}$, are those of the static compliance operator, collocated on the transducers. The factor

$$k_e L_j - 1 = \frac{L_j - 1/k_e}{1/k_e}$$

represents the apparent fraction of compliance of the whole system versus the compliance of the actuators.

Finally, the weaker the mechanical compliance of the transducers with respect to that of the system observed at the connection points is, the weaker the energy to dissipate, hence the weaker the controller set-point is.

In order to stabilize the structure at best, we should try to maximize $|\Re(s_{m_i})|$ by increasing the distance between the initial natural frequency Ω_i and the associated modified frequency ω_i (Equation (25)). This difference depends on the ratio between the system and the transducers mechanical impedances. The more the transducers stiffen the structure, the faster each pole will move toward its optimal point on the loop.

At this point, it becomes obvious that a compromise between the control levels and the stabilization levels is necessary. On the one hand, stiff transducers would fasten the damping of the mechanical modes, but at the price of a high-level energy supply. On the other hand, more flexible transducers would not necessitate a high-energy supply, but the induced modal damping will not be so high. As the IFF strategy is obviously not an optimal control strategy, some design criteria are to be defined to optimize the system. We propose the following modal criterion:

$$J_i = \frac{\Omega_i^2 - \omega_i^2}{2\Omega_i^2} \times \min_{j=1\ldots n} (k_e L_j - 1) \qquad i = 1 \ldots N \tag{36}$$

The design variables associated with the criterion are the natural pulsations of the whole structure $\Omega = \mathrm{diag}(\Omega_i)$, the modified pulsation $\omega = \mathrm{diag}(\omega_i)$ defined in Equation (25), the equivalent stiffness k_e of the transducer set-up, and the eigenvalues L_j of $k_e b^T K^{-1} b$ as defined in Equation (33).

The left-hand part $(\Omega_i^2 - \omega_i^2)/(2\Omega_i^2)$ evaluates the modal damping of the mechanical system. The right-hand part, $\min_{j=1...n}(k_e L_j - 1)$, measures the worst energy level needed to control the structure.

In addition to parameters $\{\omega_i\}_{i=1...N}$ introduced in previous work [11,26], we would like to emphasize once again the importance of the eigenvalues $\{L_j\}_{j=1...n}$.

As earlier, we can use duality to get the counterpart of these results in the case of DVF control. Then we should not use the primal basis of the substructures, but rather the dual counterpart by a method such as described in works [25,27–29]. The criterion displayed in Equation (36) can then be used directly with the design variables calculated in this dual basis.

3. ACTIVE CONTROL OF A PLATE

We now want to show how the previous results can really characterize the efficiency of IFF control on a physical system. We will apply them to damp the transversal vibrations of a plate with different sets of boundary conditions, in order to underline the control efficiency dependence on the relative ratios of structural and transducer impedances.

3.1. System description

The mechanical system considered is an aluminum plate equipped with four transducers, as displayed in Figure 4. The plate, of dimensions 350×250 mm, is 2 mm thick. Its mechanical parameters are displayed in Table I. The transducers consist of a piezoelectric force sensor and a PZT stack actuator of three 2-mm-thick layers (Table II). At each of the extremities, the actuator is sticked to a 5-mm tapped aluminum cylinder, allowing its connexion by screw. The whole set is thus connected to the plate and to its associated sensor by a surface bearing. This system has been both numerically and experimentally investigated with different boundary conditions, as mentioned above. The first system depicted in Figure 4(a) is a constrained plate connected to the transducing devices. The added embedding is localized near the connecting

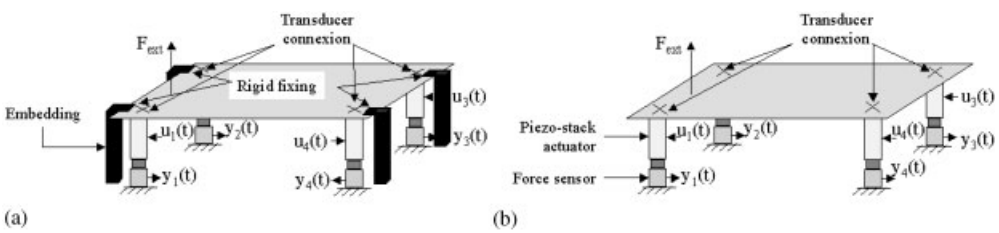

Figure 4. Scheme of mechanical test systems: (a) Constrained; and (b) non-constrained plate.

Table I. Mechanical values for the model of the plate.

Young's modulus (GPa)	70
Poisson's ratio	0.33
Density (kg m^{-3})	2700

Table II. Mechanical values for the model of the PZT stack.

Young's modulus (GPa)	10.9
Poisson's ratio	0.37
Density (kg m^{-3})	7410
ε (F m^{-1})	8.85×10^{-12}
e_{31} (N m^{-1} V^{-1})	14
e_{32} (N m^{-1} V^{-1})	14
e_{33} (N m^{-1} V^{-1})	54.5

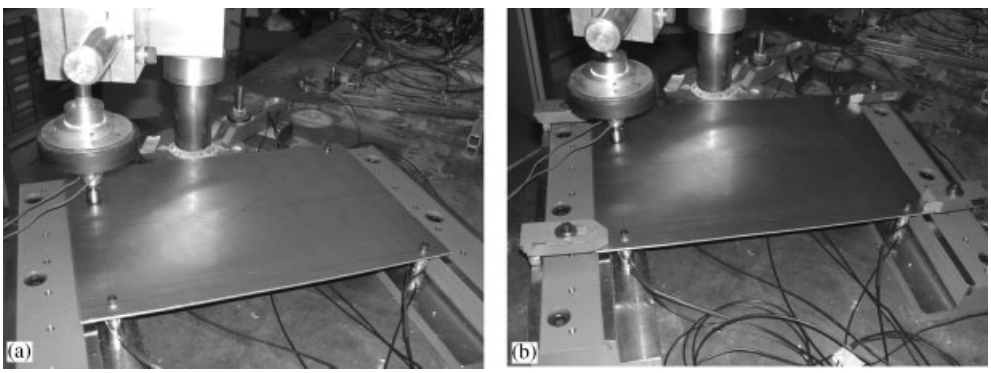

Figure 5. Experimental set-up: (a) Non-constrained; and (b) constrained plate.

points between the plate and the active device as shown in Figure 4(b). The second is a free plate connected to the same transducers. The experimental set-up is shown on Figure 5.

3.2. Modeling of the systems

The sensor has been modeled with multi-physical finite-elements coupling piezo-mechanics and electro-statics, using the Femlab© software. Reduced mass and stiffness matrices have been obtained by a Guyan reduction of the initial matrices. The final matrices are that of a classical beam model with five degrees of freedom per node (without torsion). The force measurement matrix has been calculated directly using the sensor longitudinal stiffness.

The piezoelectric stack actuator and the connexion cylinder have been modeled by multi-physical finite elements to take the piezoelectric coupling effect into account. As earlier, the mass, stiffness and reciprocal piezoelectric coupling (between the applied voltage and the induced mechanical stress) have been obtained by a simple static Guyan reduction. The resulting matrices are as previously that of a beam model with five degrees of freedom per node.

The plate was simply modeled by two-dimensional plate elements. Its mass, stiffness and external force matrices have been calculated by a global Craig–Bampton condensation. In order to model correctly the inner dynamics of the structure, fifty vibration modes have been taken into consideration. In-plate rotation has been suppressed from the model.

3.3. Control tests

The IFF strategy has been implemented with three different control architectures. For each one, the feedback matrix has been appropriately modified.

Control case 1. This control uses only one transducer (Figure 6). For symmetry reasons, we can choose any transducer of the system. It allows us to quantify the individual efficiency of the transduction system.

Control case 2. We now use all transducers in a parallel, fully decentralized version (Figure 7). The set-point of each transducer will be effectively independent of the measurements of the other ones.

Control case 3. This strategy allows us to target the efficiency of the control at several modes of the structure. We try here to control only the symmetric or antisymmetric modes with respect to the symmetry axes of the plate. For this purpose, we introduce the shape matrix Q in the feedback loop, which will vary according to the targeted mode(s) (Table III). The control is now centralized (Figure 8).

This very classical strategy can be extended to the notion of modal filter [30,31] and allows a selective sorting of the controlled modes. In our particular case, the modal selective filtering of the four first modes is not possible, because the transducers are symmetrically placed on the plate with respect to both symmetrical axes, which singularizes the modal participation matrix reduced to the four first modes: the transducers cannot distinguish mode 1 from mode 4.

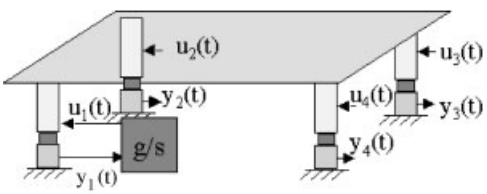

Figure 6. Application scheme of control type 1.

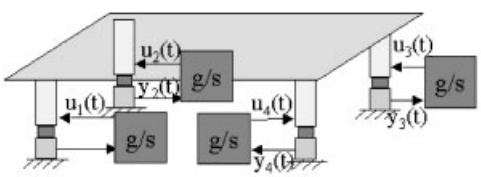

Figure 7. Application scheme of control type 2.

Table III. Different filters to target the control to some choosen modes.

Filter type	Targetted mode description	Matrix form
Filter 1	Symmetrical modes with respect to x and y	$Q^{\mathrm{T}} = [1\ 1\ 1\ 1]$
Filter 2	Antisymmetrical modes with respect to y	$Q^{\mathrm{T}} = [1\ 1\ -1\ -1]$
Filter 3	Antisymmetrical modes with respect to x	$Q^{\mathrm{T}} = [1\ -1\ -1\ 1]$
Filter 4	Antisymmetrical modes with respect to x and y	$Q^{\mathrm{T}} = [1\ -1\ 1\ -1]$

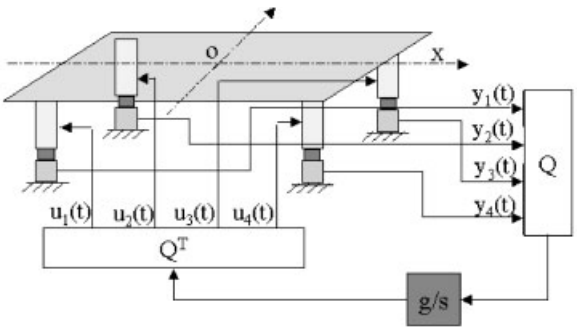

Figure 8. Application scheme of control type 3.

Feedback matrix G is now a full matrix:

$$G = Q\frac{g}{s}I_n Q^{\mathrm{T}}$$

We can however use the previously defined design criterion by using a modified influence vector such that $b \leftarrow bQ$.

3.4. *Experiment*

Figure 5 depicts the experimental set-up in case of constrained (b) and non-constrained plate (a). The plate is excited by a magnet coil. A collocated accelerometer allows to measure the global efficiency of the control. The perturbation and the measurement of the sensor voltage are performed with a Siglab© platform. The control law is implemented experimentally via a DSpace© platform, which enables to modify the feedback gain interactively. For each set of tests, the transfer function between the perturbation and the accelerometer has been drawn to observe any modal peak decrease.

4. CONTROL OF A CONSTRAINED PLATE

The first series of tests has been conducted on a constrained plate. Table IV displays the ten first natural frequencies of the whole mechanical system. It also gather the modal damping that has been achieved experimentally with different configuration that will be further discussed.

4.1. *Decentralized control with one transducer (control case 1)*

The numerical root locus associated to this control is displayed on Figure 9. It displays the mechanical poles of the plate, each one moving on a loop going to a zero of the SISO system.

As the open-loop poles and zeros are not well separated, the loops do not deepen far in the left half plane and the induced stabilization is reduced. It leads to some small maximal modal damping, peaking at 0.6% for the first and second modes.

Figure 10 displays the values of the modal efficiency criterion $J_i \times 10^6$ proposed in Equation (36). By comparing it with Figure 9, we can check the agreement between the depth of a loop and the size of the corresponding bar.

Table IV. Damping achieved on the constrained plate.

Mode	Frequency (Hz)	Damping Ratio (%)		
		Without control	With one transducer	With all transducers
1	81.6	0.64	1.51	5.66
2	138.1	0.40	1.20	4.42
3	169.3	1.69	2.30	2.87
4	187.9	0.61	0.88	1.30
5	278.1	1.29	1.30	1.34
6	285.3	0.92	1.19	1.81
7	314.2	0.25	0.23	1.02
8	333.5	0.28	1.06	1.59
9	408.2	1.17	1.29	2.75
10	436.7	0.97	1.36	1.25

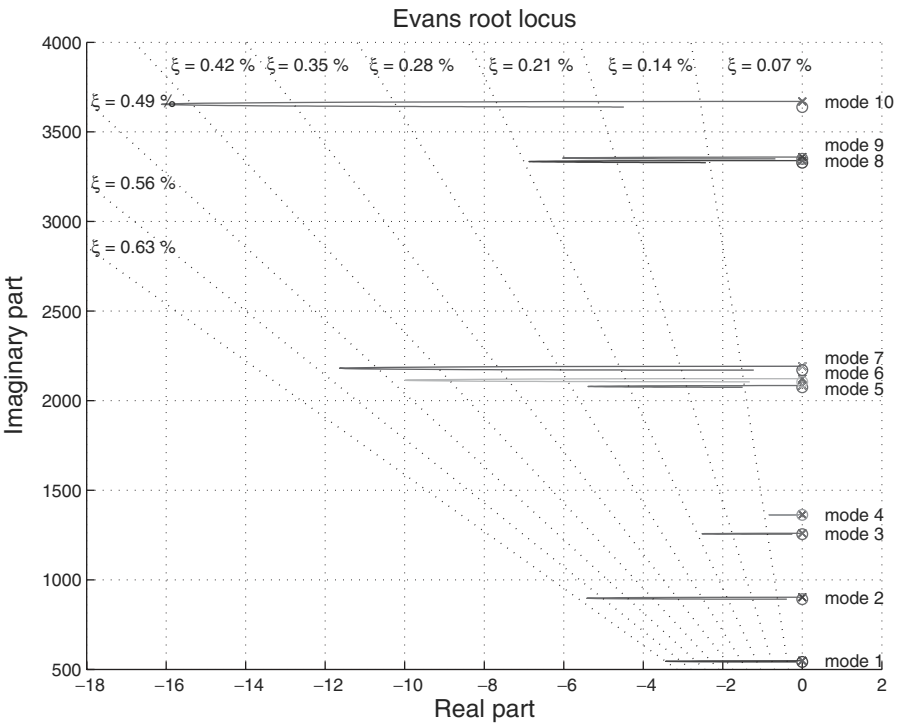

Figure 9. Evans root locus: mechanical modes (−) and zeros.

Experimentally, a control voltage of 57 V RMS has been necessary to achieve the damping ratios displayed in Table IV. These results are better than what the numerical maximal damping ratio values had suggested.

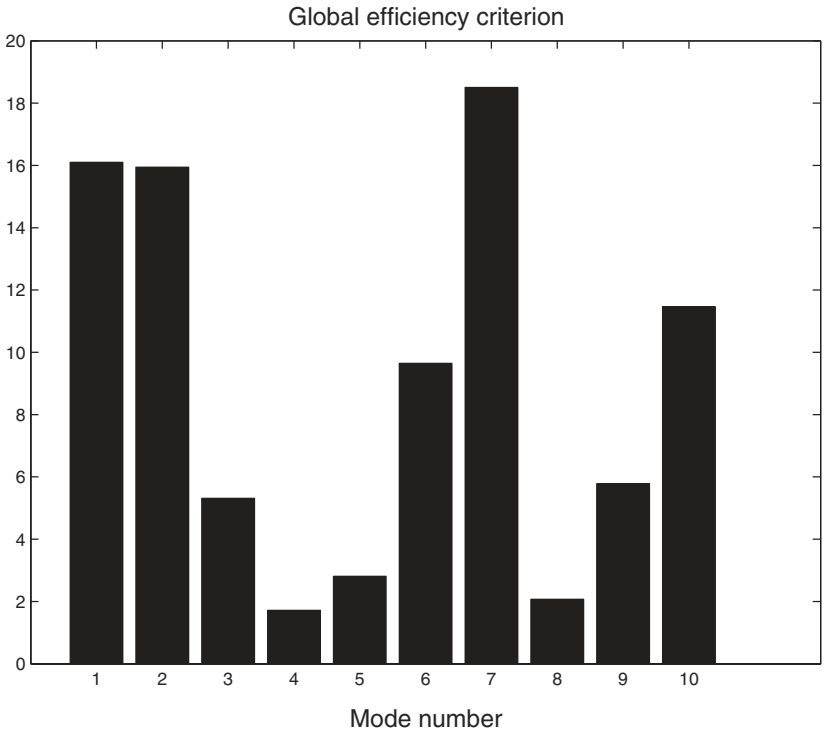

Figure 10. Modal efficiency criterion J_i ($\times 10^6$).

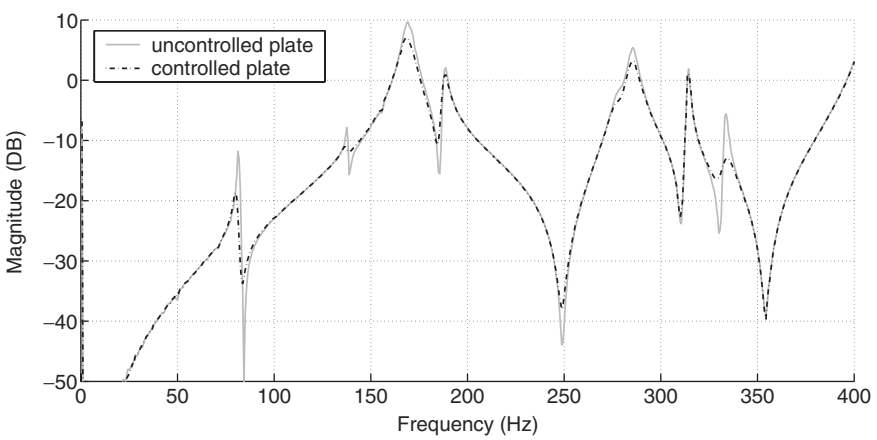

Figure 11. FRF between excitation and collocated accelerometer.

4.2. Decentralized control with all transducers (control case 2)

The root locus associated with the control with all transducers can be found on Figure 12. The loops associated with the mechanical poles deepen further in the left half-plane than those

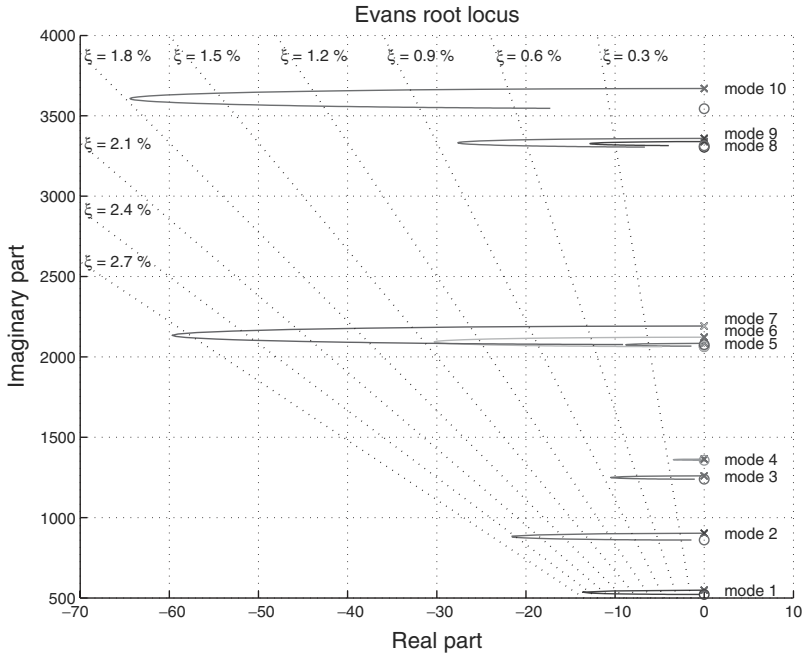

Figure 12. Evans root locus: mechanical modes (×) and zeros (◦).

obtained for the control with only one transducer, resulting in a higher achievable damping. As the poles and zeros remain close to each other, this damping is not very high anyway. It does not exceed 2.6% for the first mode, what is however four times greater than the factor of control case 1.

The values given by the modal criterion $J_i \times 10^6$ (Figure 13) show a four-fold increase compared with the case with only one transducer.

The efficiency of this control can be verified experimentally, again (Table IV): the RMS control voltage decreases from 57 to 29 V. At the same time, we observe a higher decrease of the magnitude peaks (Figure 14).

4.3. Centralized control (control case 3)

Figure 15 shows the evolution of modal damping of the first seven mechanical modes with respect to the gain feedback g, with the four centralized architectures defined in Table III. We observe a decoupling for those modes which are sensitive to the control.

By comparing Figure 15 with Figure 12, we do not notice any increase due to filtering in the maximal potential modal damping. Similarly, if we compare the magnitude decrease of the first modal peaks on Figures 11 and 16, we do not notice any improvement. However, if we measure the RMS voltage needed to control the system, we get a smaller value: 24 instead of 29 V. This decentralized architecture is thus more efficient than the centralized one.

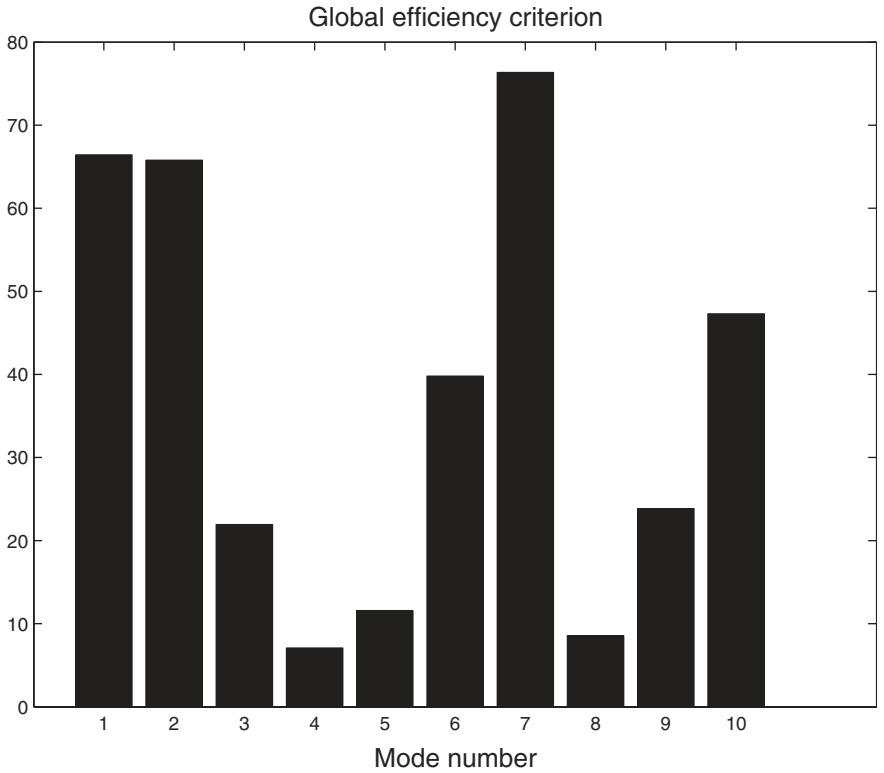

Figure 13. Modal efficiency criterion J_i ($\times 10^6$).

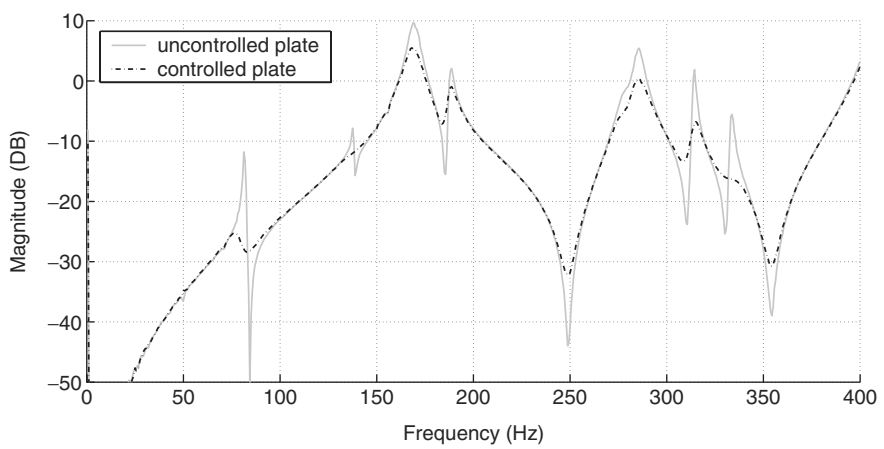

Figure 14. FRF between excitation and collocated accelerometer.

5. CONTROL OF A FREE PLATE

To underline the relevance of our design criterion J_i, a second series of tests has been conducted on a free plate.

5.1. Decentralized control with one transducer (control case 1)

The root locus associated with this control is displayed in Figure 17. The mechanical poles move on the same trajectories than that described previously. However, as poles and zeros are well separated, these loops are far wider as those on Figure 9. This leads to high potential damping factors, particularly for the first mode (12%) and the third mode (16%).

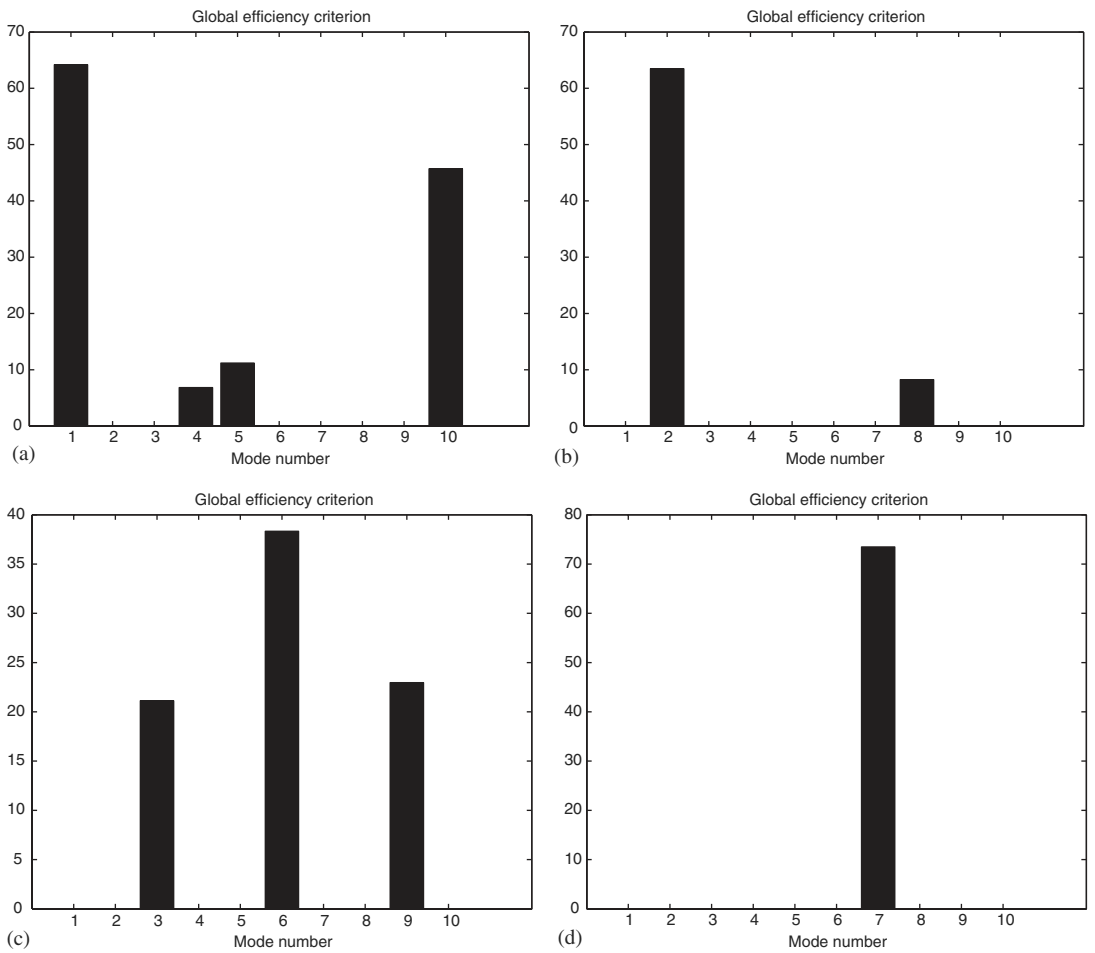

Figure 15. Evolution of the modal criterion for the first 10 modes with different control architectures, each targeted on some specific modes: (a) Filter 1; (b) filter 2; (c) filter 3; and (d) filter 4.

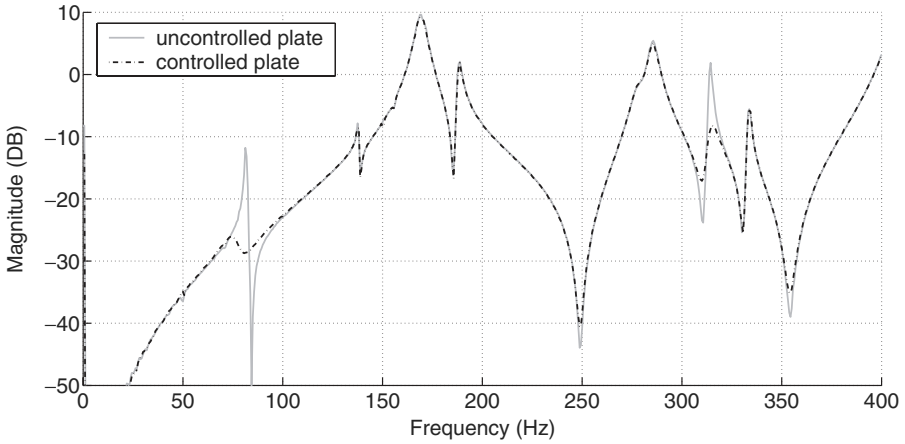

Figure 16. FRF between excitation and collocated accelerometer with filter 1.

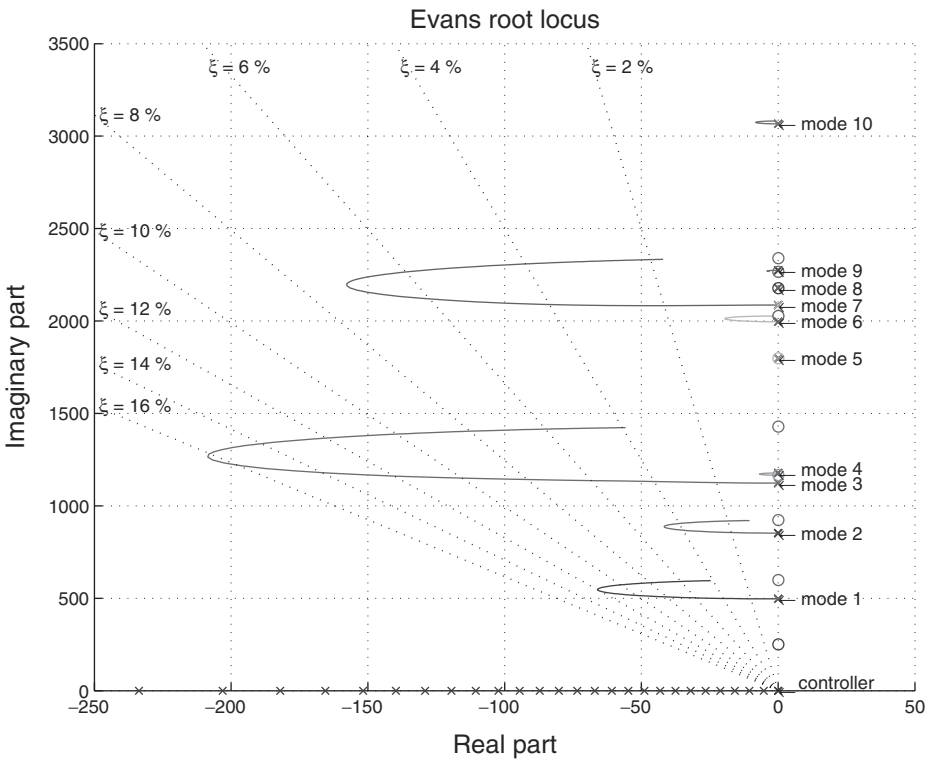

Figure 17. Root locus and localization of zeros.

Figure 18 shows the values of our modal efficiency criterion $J_i \times 10^6$ for the first 15 natural frequencies. The values obtained are of the order of 100 times smaller than those calculated for the constrained system (Figure 10). They predict that suppressing the restraints in the system has

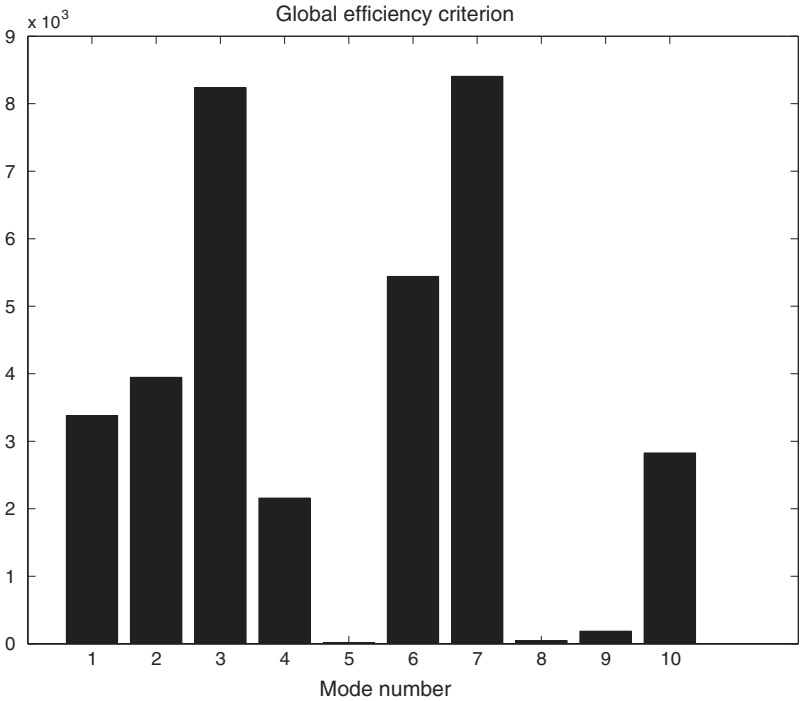

Figure 18. Modal efficiency criterion J_i ($\times 10^6$).

Table V. Damping achieved on the free plate.

		Damping Ratio (%)		
Mode	Frequency (Hz)	Without control	With one transducer	With all transducers
1	70.8	0.89	1.57	1.68
2	126.9	1.43	1.32	1.61
3	132.3	2.48	3.06	3.39
4	168.7	0.56	0.46	1.04
5	217.9	2.69	2.76	2.70
6	253.3	3.02	2.38	2.87
7	288.3	1.50	1.31	1.55
8	302.4	0.52	0.58	0.57
9	353.3	2.85	2.54	2.75
10	378.5	1.61	1.67	2.19

worsen efficiency, even if the maximal eligible damping values have been highly increased. So we cannot expect good results for this strategy.

Experimental tests confirm the low efficiency of this control (Table V). Actually, it does not enable one to decrease significantly the magnitude of the modal peaks of the structure (Figure 19), for the same control voltage (57 V RMS) than previously. Thus, these results confirm the relevance of our criterion.

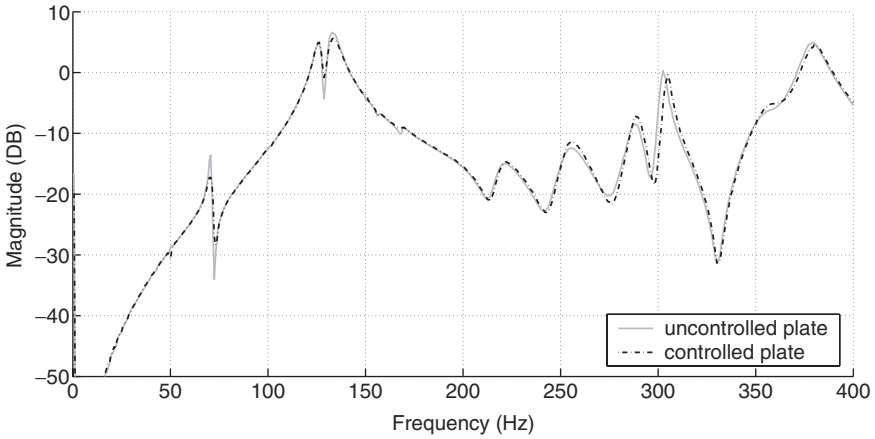

Figure 19. FRF between excitation and collocated accelerometer.

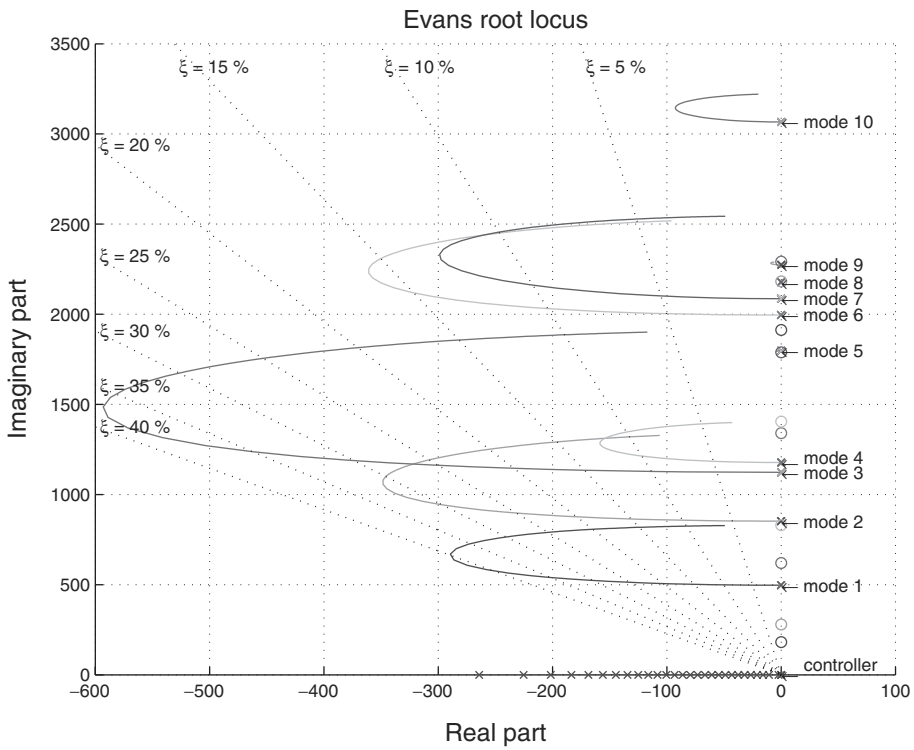

Figure 20. Evans root locus: mechanical poles (+) and zeros (◦).

5.2. *Decentralized control with all transducers (control case 2)*

The root locus associated with this control can be found in Figure 20. The loops associated with the mechanical poles are very wide, which translates into very high damping coefficients: around

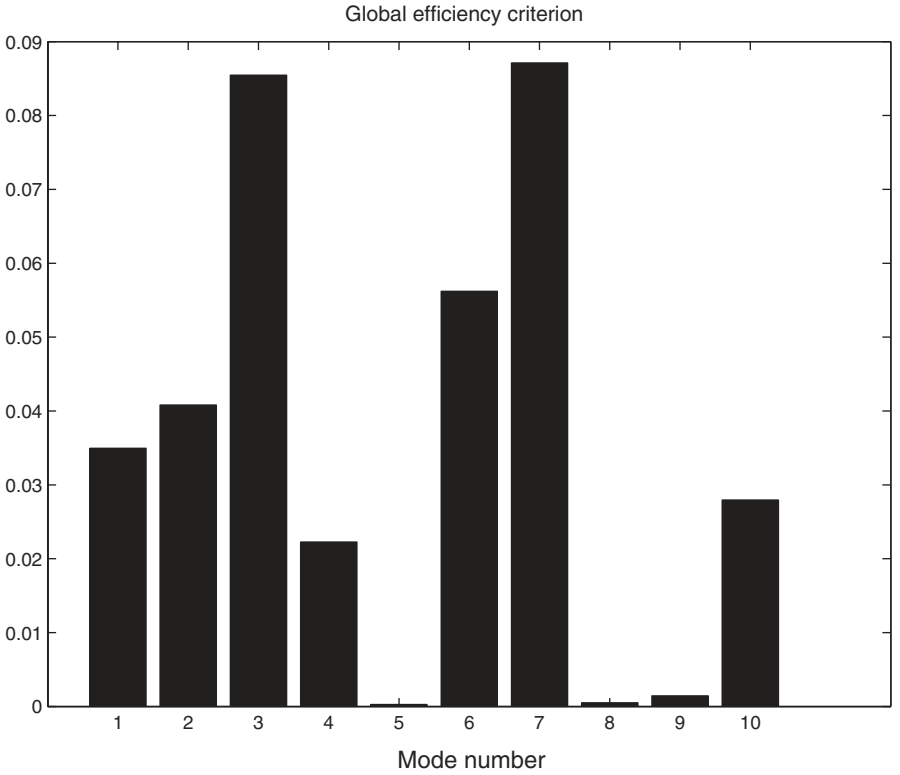

Figure 21. Modal efficiency criterion J_i ($\times 10^6$).

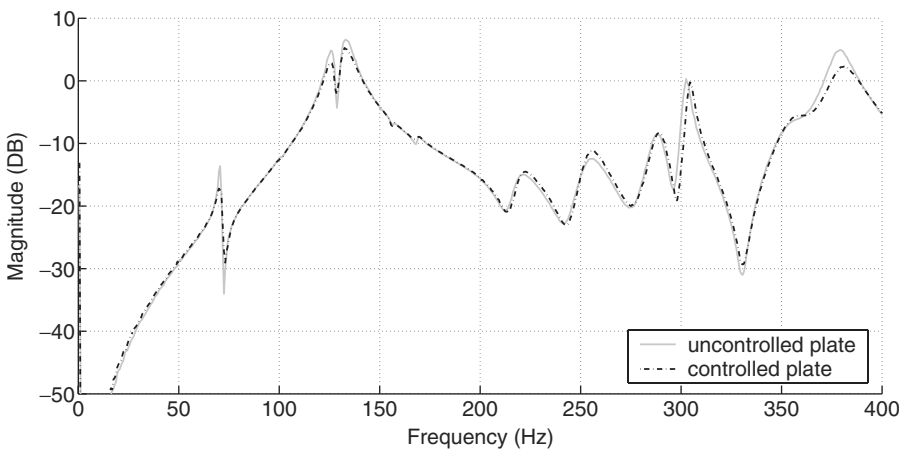

Figure 22. FRF between excitation and collocated accelerometer.

40% on modes 1 and 3. The diagram displayed in Figure 21 shows the values of the design criterion $J_i \times 10^6$. We notice that they are even smaller than the previous ones.

As previously mentioned, this control strategy does not have any additional impact on the modal damping of the system. Indeed, Figure 22 does not show any significant diminution in

magnitude compared with the system controlled with only one transducer (Figure 19). Table V summarizes the improvement in modal damping for the two previous cases.

At this step, we can notice that numerical simulations and experimental analysis are in complete agreement with our initial theoretical reflexion. Even if the control of the plate with this architecture leads to potentially very high modal damping factors, the energy level that should be supplied to the system is so high that the maximal damping is finally unattainable in practice. The decentralized IFF strategy associated with these stiff transducers is here completely inefficient to stabilize the structure.

6. CONCLUSIONS AND FURTHER DEVELOPMENTS

This work has allowed us to demonstrate a complete criterion (Equation (36)) made from simple design parameters, enabling us to optimize IFF efficiency. Both numerical and experimental investigations have shown the relevance of such an efficiency measurement. This proposed tool complements and states precisely the previous one proposed in [11]. By computing only two sets of specific eigenvalues, any transducer set-up can be optimized to increase the damping effect induced by the IFF strategy while keeping the energy consumption at a minimum. The proposed numerical tool is generic and can be used for any structure and any system of transduction as far as IFF or DVF is concerned.

Furthermore we have also shown the improvement of modal efficiency that can be obtained by a centralized approach. Much more intricate, this method can, on the other hand, allow one to achieve a maximum damping by using a smaller actuator signal than with a decentralized approach.

Thanks to its simplicity, this criterion can be applied to industrial systems that are hard to control. To further improve efficiency, we can try to optimize the system in two ways. First, some modified control laws could be considered, aiming at maximizing the maximum damping ratios by separating the mechanical poles and zeros as seen by the controller. Thus, the feedback compensation law introduced in [32] is worth investigation. Another strategy could be to optimize the filtering matrix Q. Second, the transducers should be optimized so that their stiffness be adapted with that of the mechanical system to be controlled.

REFERENCES

1. Xiongzhu Bu, Lin Ye, Zhongqing Su, Chunhui Wang. Active control of a flexible smart beam using a system identification technique based on armax. *Smart Material and Structures* 2003; **12**:845–850.
2. Pan X, Hansen CH. Effect of end conditions on the active control of beam vibration. *Journal of Sound and Vibration* 1993; **168**:429–448.
3. Petersen IR, Pota HR. Minimax lqg optimal control of a flexible beam. *Control Engineering Practice* 2003; **11**: 1273–1287.
4. Lagnese J, Lions J-L. *Contrôle des plaques*. Masson: Paris, 1992.
5. Chattopadhyay A, Seeley CE, Jha R. Aeroelastic tailoring using piezoelectric actuation and hybrid optimization. *Smart Material and Structures* 1999; **8**:83–91.
6. Lam TY, Ng KY. Active control of composite plates with integrated piezoelectric sensors and actuators under various dynamic loading conditions. *Smart Material and Structures* 1999; **8**:223–237.
7. Saravanan C, Ganesan N, Ramamurti V. Semianalytical finite element analysis of active constrained layer damping in cylindrical shells of revolution. *Computers and Structures* 2001; **79**:1131–1144.

8. Pinto Correia IF, Mota Soares CM, Mota Soares CA, Herskovits J. Active control of axisymmetric shells with piezoelectric layers: a mixed laminated theory with a high order displacement field. *Computers & Structures* 2002; **80**:2265–2275.
9. Meirovitch L, Baruth H. On the robustness of independent modal-space control method. *Journal of Guidance Control and Dynamics* 1983; **6**:20–25.
10. Balas MJ. Feedback control of flexible systems. *IEEE Transactions on Automatic Control* 1978; **23**:673–679.
11. Preumont A. *Vibration Control of Structures*: *An Introduction*. Kluwer: Dordrecht, 1997.
12. Ozbay H. *Feedback Control Theory*. CRC Press: Boca Raton, 2000.
13. El Ghaoui L, Niculescu S-I (eds). *Advances in Linear Matrix Inequality Methods in Control*, *Advances in Design and Control*, vol. 2, Society for Industrial and Applied Mathematics (SIAM): Philadelphia, 2000.
14. Lim KB. Robust control on vibrating structures. In *Responsive Systems for Active Vibration Control*, Preumont A (ed.), vol. 85. *NATO Science Programme*. Kluwer: Dordrecht, 2002; 133–179.
15. Lions J-L. Exact controllability, stabilization and perturbations for distributed systems. *SIAM Review* 1988; **30**:1–68.
16. Komornik V. Rapid boundary stabilization of linear distributed systems. *SIAM Journal of Control and Optimization* 1997; **35**(5):1591–1613.
17. Bourquin F, Briffaut J-S, Collet M. On the feedback stabilization: Komornik's method. In *Proceedings of the 2nd International Symposium on Active Control in Mechanical Engineering*, Lyon, France, 1997.
18. Bourquin F, Collet M, Ratier L. Modeling and numerical issues for the control of flexible structures. In *Proceedings of the 3rd International Workshop on Structural Control*, Magonette G, Casciati F (eds). World Scientific: Singapore, 2000.
19. Bourquin F, Briffaut JS, Collet M, Joly M, Ratier L. Fast control algorithms for beams: experimental results. *Proceedings of Forum Acousticum*, Berlin, 1999.
20. Balas MJ. Direct velocity feedback control of large space structures. *Journal of Guidance and Control Engineering Notes* 1979; **2**(3):252–253.
21. Ehmann C, Nordmann R. Comparison of control strategies for active vibration control of flexible structures. *Proceedings of the 6th Conference on Active Noise and Vibration Control Methods*, Cracow, Poland, 2003.
22. Holterman J, de Vries TJA. Self-tuning integral force feedback. In *Proceedings of the 5th International Conference on Motion and Vibration Control*, Samali B (ed.). Sydney, Australia, 2000; 643–648.
23. Holterman J, de Vries TJA. Prediction and improvement of the maximum achievable damping with collocated control. *Proceedings of the Tenth International Congress on Sound and Vibration*, Stockolm, Sweden, 2003.
24. Achkire Y, Bossens F, Preumont A. Active damping and flutter control of cable-stayed bridges. *Journal of Wind Engineering and Industrial Aerodynamics* 1998; **74–76**:913–921.
25. Rixen DJ. Dual schur complement method for semi-definite problems. *Contemporary Mathematics* 1998; **218**: 341–348.
26. Achkire Y, Preumont A. Active damping of structures with guy cables. *Actes de l'Ecole CEA EDF INRIA sur les matériaux intelligents*, 1997.
27. Farhat C, Lesoinne M, Pierson K. A scalable dual-primal domain decomposition method. *Numerical Linear Algebra with Applications* 2000; **7**:687–714.
28. Klawonn A, Widlund OB. Dual and dual-primal FETI method for elliptic problems with discontinuous coefficients in three dimensions. In *Proceedings of the 12th International Conference on Domain Decomposition Methods*, Chan T, Kako T, Kawarada H, Pironneau O (eds). 2001.
29. Pierson KH, Reese GM, Raghavan P. Experiences with FETI-DP in a production level finite element application. In *Fourteenth International Conference on Domain Decomposition Methods*, Herrerra I, Keyes DE, Widlund OB, Yates R (eds). DDM.org, 2003.
30. Collet M, Jézéquel L. Active control with piezoelectric layers optimization. *Journal of Structural Control* 1995; **1**:59–79.
31. Collet M. Shape optimization of piezoelectric sensors dealing with spill-over instabilities. *IEEE Transactions on Control System Technology* 2001; **9**(4):654–663.
32. Holterman J, de Vries TJA. Active damping within an advanced microlithography system using piezoelectric smart discs. *Mechatronics* 2003; **13**.